




ARTICLE

Variants in *ADD1* cause intellectual disability, corpus callosum dysgenesis, and ventriculomegaly in humans



Cai Qi¹, Irena Feng¹, Ana Rita Costa², Rita Pinto-Costa², Jennifer E. Neil³, Oana Caluseriu⁴, Dong Li⁵, Rebecca D. Ganetzky^{6,7}, Charlotte Brasch-Andersen⁸, Christina Fagerberg⁸, Lars Kjærsgaard Hansen⁸, Caleb Bupp⁹, Colleen Clarke Muraresku^{6,7}, Xiangbin Ruan¹, Bowei Kang¹, Kaining Hu¹, Rong Zhong¹, Pedro Brites¹⁰, Elizabeth J. Bhoj⁵, Robert Sean Hill³, Marni J. Falk^{6,7}, Hakon Hakonarson^{5,7}, Kristopher T. Kahle¹¹, Monica M. Sousa^{2,*}, Christopher A. Walsh^{3,**}, Xiaochang Zhang^{1,12,***} 

ARTICLE INFO

Article history:

Received 25 May 2021

Revised 24 August 2021

Accepted 21 September 2021

Available online 30 November 2021

Keywords:

Adducin

Alternative splicing

Axon degeneration

Membrane-associated periodic

ring-like structure (MPS)

ABSTRACT

Purpose: Adducins interconnect spectrin and actin filaments to form polygonal scaffolds beneath the cell membranes and form ring-like structures in neuronal axons. Adducins regulate mouse neural development, but their function in the human brain is unknown.

Methods: We used exome sequencing to uncover *ADD1* variants associated with intellectual disability (ID) and brain malformations. We studied *ADD1* splice isoforms in mouse and human neocortex development with RNA sequencing, super resolution imaging, and immunoblotting. We investigated 4 variant *ADD1* proteins and heterozygous *ADD1* cells for protein expression and *ADD1*–*ADD2* dimerization. We studied *Add1* functions in vivo using *Add1* knockout mice.

Results: We uncovered loss-of-function *ADD1* variants in 4 unrelated individuals affected by ID and/or structural brain defects. Three additional de novo copy number variations covering the *ADD1* locus were associated with ID and brain malformations. *ADD1* is highly expressed in the neocortex and the corpus callosum, whereas *ADD1* splice isoforms are dynamically expressed between cortical progenitors and postmitotic neurons. Human variants impair *ADD1* protein expression and/or dimerization with *ADD2*. *Add1* knockout mice recapitulate corpus callosum dysgenesis and ventriculomegaly phenotypes.

Conclusion: Our human and mouse genetics results indicate that pathogenic *ADD1* variants cause corpus callosum dysgenesis, ventriculomegaly, and/or ID.

© 2021 American College of Medical Genetics and Genomics.

Published by Elsevier Inc. All rights reserved.

*Correspondence and requests for materials should be addressed to Monica M. Sousa, Nerve Regeneration Group, University of Porto, Rua Alfredo Allen 208, 4200135, Porto. E-mail address: msousa@ibmc.up.pt

**Correspondence and requests for materials should be addressed to Christopher A. Walsh, Boston Children's Hospital and Harvard Medical School, Center of Life Sciences 15th floor, 3 Blackfan Circle, Boston, MA 02115. E-mail address: christopher.walsh@childrens.harvard.edu

***Correspondence and requests for materials should be addressed to Xiaochang Zhang, Department of Human Genetics and The Grossman Institute for Neuroscience, The University of Chicago, 920 E 58 St. CLSC Room 507A, Chicago, IL 60637. E-mail address: xczhang@uchicago.edu

Affiliations are at the end of the document.

Introduction

The corpus callosum connects corresponding cortical areas of the left and right cerebral hemispheres in mammals, and agenesis/dysgenesis of the corpus callosum is associated with intellectual disability (ID) and speech delay.^{1,2} The generation of the corpus callosum occurs early in development and is critical for the functional synchronization of the 2 hemispheres.³ Corpus callosum malformation is the most frequently observed structural brain defect,^{4,5} often caused by abnormal neurogenesis, migration, and axon guidance.²

Three adducin genes, namely *ADD1*, *ADD2*, and *ADD3*, encode cytoskeleton proteins that are critical for osmotic rigidity and cell shape.^{6,7} Adducins are best known for their association with the junctional complex in erythrocytes, interconnecting spectrin and actin filaments to form polygonal scaffolds beneath the cell membrane.^{8,9} In neurons, adducins have been reported to form a membrane-associated periodic ring-like structure (MPS) with actin and β -spectrin,¹⁰ and our previous work showed that deletion of *Add1* in mice led to an increase in the diameter of the MPS rings and axonal degeneration.¹¹

ADD1, *ADD2*, and *ADD3* form heterodimers (*ADD1/ADD2*, *ADD1/ADD3*), which further form heterotetramers.¹² *ADD1* and *ADD3* are expressed in most tissues, whereas *ADD2* is highly expressed in the brain and erythrocytes.⁷ The 3 adducins have similar protein structures consisting of the following 3 main domains: the head, neck, and tail domains. The C-terminal tail domain has a well-conserved MARCKS-related domain that targets adducins to lateral membranes and stimulates β -spectrin–actin association.^{13,14}

In *Add1* null mice, *ADD2* and *ADD3* proteins were also undetectable,^{11,15} indicating a predominant role of *ADD1* in stabilizing *ADD2* and *ADD3*. *Add1* null mice showed growth retardation and anemia and approximately 50% developed lethal communicating hydrocephalus accompanied by dilation of the ventricles.¹⁵ Moreover, *ADD1* regulates synaptic plasticity through glutamate receptors and is associated with memory performance in humans.¹⁶ In contrast, *Add2* knockout (KO) mice did not show structural brain malformation and had increased *ADD1/ADD3* protein levels in the membrane fraction, suggesting dosage compensation.^{17,18} *Add2* regulates activity-dependent connectivity formation, and *Add2* KO was reported to impair spine turnover in hippocampal neurons.^{19,20}

In this study, we report 4 *ADD1* variants associated with neurological symptoms, including 1 recessive missense variant and 3 de novo variants. The recessive variant is associated with absence of the corpus callosum and enlarged lateral ventricles, and the de novo variants are associated with variable degrees of neurological disorders ranging from complete or partial agenesis of corpus callosum (ACC) to mild ID and attention deficit. We show that alternative splicing generates different isoforms of *ADD1* between

neural progenitors and cortical neurons, and *ADD1* variants impair normal protein function. In addition to the previously reported lethal hydrocephaly phenotypes, *Add1* KO mice that survived showed reduced thickness of the corpus callosum in adulthood. Our human and mouse genetic results indicate that *ADD1* loss-of-function (LoF) is associated with corpus callosum malformation, ventriculomegaly, and/or ID.

Materials and Methods

Molecular cloning

For ectopic expression of genes in the neuronal system, the pCAGIG (Addgene, 11159) vector and its previously described derivatives²¹ were used in this study. *ADD1* and *ADD2* genes were amplified using polymerase chain reaction (PCR) and inserted into the *AscI*- and *NotI*-digested pCAG-HA-Flag-IRES-GFP and pCAG-V5-Flag-IRES-GFP vectors, respectively. *Ptbp1* short hairpin RNA (shRNA) knockdown constructs were as reported previously.²¹

Immunoprecipitation

Immunoprecipitation was carried out using anti-HA Magnetic Beads as instructed by the manufacturer (Thermo Fisher Scientific, 88837). Wild-type and mutated *ADD1* coding sequences were subcloned into the pCAG-HA-Flag-IRES-GFP vector, and *ADD2* was subcloned into the pCAG-V5-Flag-IRES-GFP vector. Then, different versions of mutated *ADD1* and *ADD2* were co-transfected into HEK293FT cells. After 36 to 48 hours of transfection, cells were lysed with Pierce IP Lysis Buffer (Thermo Scientific, 87787), and 500 μ g lysate was used for immunoprecipitation with anti-HA magnetic beads for 30 minutes at room temperature. The immunoprecipitated protein was denatured and subjected to western blotting.

RNA and protein analysis

DNase-treated total RNA samples were reverse transcribed using SuperScript IV with random hexamers following manufacturer's instructions (Invitrogen, 18-090-050), diluted, PCR amplified (primer sequences in [Supplemental Table 1](#)), and resolved on agarose gels. Protein lysates were resolved using sodium dodecyl sulfate–polyacrylamide gel electrophoresis gels, and western blots were carried out using the LI-COR Odyssey system. For immunofluorescence staining, embryonic mouse brains were dissected, fixed in 4% paraformaldehyde overnight at 4 °C, and cryopreserved in 30% sucrose. Coronal sections were stained with primary antibodies at 4 °C overnight and then with secondary antibodies for 1 hour at room temperature. The

primary antibodies used in this study are listed in [Supplemental Table 2](#).

Cell culture and generation of KO cells

HEK293FT cells were cultured in DMEM supplemented with 10% fetal bovine serum. Cells were transfected with single guide RNAs and seeded into 10 cm culture dishes (1000 cells per dish). Single colonies were picked 7 to 10 days later and cultured in 96-well plates for genotyping using Sanger sequencing. The ones with no variants were used as wild-type controls, whereas the ones containing variants were used as mutated cell lines.

Exome sequencing and data analysis

For case I, genomic DNA was extracted from peripheral blood and subjected to array capture with the SureSelect Human Exon Kit (Agilent). Seventy-six base pair paired-end sequencing was performed on an Illumina HiSeq 2000 at the Broad Institute, yielding ~10 Gb of sequences per sample covering 86% of the target sequence at least 20 times. Sequencing reads were trimmed and aligned to the reference human genome (hg19) with the Burrows-Wheeler Aligner (v.0.5.7), followed by variant calling with the Genome Analysis Toolkit and variant annotation with ANNOVAR. Annotated variants were entered into a MySQL database and filtered with custom queries. Exome sequencing of other cases and their parents was performed following comparable procedures and filtered for de novo variants.

Analysis of alternatively spliced exons

Analysis of alternative splicing was performed as reported previously.²¹ RNA sequencing data sets of laser micro-dissected cortical tissues²² were reanalyzed, and Sashimi plots were generated in the Integrative Genomics Viewer.²³ To validate differentially-spliced adducin exons during human brain development, we microdissected gestational week (GW) 15, GW17, and GW18 fetal human cortical tissues and performed reverse transcriptase-PCR (RT-PCR). We also harvested dorsal brain tissues from embryonic day (E) 12.5, E14.5, E16.5, E18.5, postnatal day (P) 12, and P40 CD1 mice, and extracted RNA with TRIzol (Sigma-Aldrich) for RT-PCR.

Hippocampal neuron culture

Mouse and rat hippocampal neuron cultures were performed as previously described.²⁴ Briefly, hippocampi on E18.5 were digested in 0.06% trypsin from porcine pancreas solution for 15 minutes (Sigma-Aldrich, T4799) and triturated. A total of 12,500 cells per coverslip were plated onto 50 µg/mL poly-L-lysine hydrobromide (Sigma-Aldrich,

P2636-100MG) precoated 1.5H glass 13 mm rounded coverslips (Paul Marienfeld GmbH & Co KG) in 24-well plates (Nunc). Neurons were then cultured in Neurobasal Medium (Thermo Fisher Scientific, 21103-049) supplemented with 2% B-27 Supplement (50×) (Thermo Fisher Scientific, 0080085SA), 1% Penicillin-Streptomycin (10,000 U/mL) (Thermo Fisher Scientific, 15140-122), and 2 mM L-glutamine (200 mM) (Thermo Fisher Scientific, 25030024).

Immunostaining

Primary hippocampal neurons were fixed after 10 days in vitro with 4% paraformaldehyde (in phosphate-buffered saline [PBS] at pH 7.4) for 20 minutes at room temperature. Fixed cells were permeabilized with 0.1% (v/v) Triton X-100 (in PBS) for 5 minutes, quenched with 0.2 M ammonium chloride (Merck, 1.01145.0500), and incubated with blocking buffer (5% fetal bovine serum in PBS) for 1 hour. Primary antibodies diluted in blocking buffer were incubated overnight at 4 °C ([Supplemental Table 2](#)). After three 5-minute washes in PBS, secondary antibodies were incubated for 1 hour at room temperature. Images were acquired using a TCS Leica SP8 confocal microscope.

Stimulated emission depletion (STED) imaging

Stimulated emission depletion imaging was performed on an Expert Line gated-STED (Abberior Instruments) coupled to a Ti microscope (Nikon). Ten days in vitro hippocampal neurons were imaged at a fixed distance of 80 to 100 µm from the cell body with an oil-immersion 60× 1.4NA Plan-Apo objective (Nikon, Lambda Series) using confocal and STED modes. The system featured 40 MHz modulated excitation (405, 488, 560, and 640 nm) and depletion (775 nm) lasers. The microscope's detectors were avalanche photodiode detectors. The 2-dimensional vortex STED images with lateral resolution enhancement were recorded with 20 nm pixel size in XY, and the pinhole was set to 0.8 Airy units. To analyze ring periodicity, the maximum intensity of peaks was determined and the interpeak distance was measured.

Animals

Add1 KO mice and wild-type littermates (129S1/SvImJ;C57BL/6J) were obtained from heterozygous breeding pairs and genotyped as described.¹⁵ The protocols described were approved by of the University of Chicago Institutional Animal Care and Use Committee and/or the Instituto de Biologia Molecular e Celular (IBMC) ethical committee and by the Portuguese Veterinarian Board. Brains from P0, P14, and adult (9-week-old) animals were collected and fixed with 4% paraformaldehyde for 24 hours at 4 °C. After dehydrating and clearing in toluene, brains were embedded in paraffin, and whole brain coronal

sections with a thickness of 6 μm were cut using Microm HM335E Microtome (GMI-Trusted Laboratory Solutions). Cuts from 2 different regions of the corpus callosum (planes 27-30 and 41-50, according to the Allen Mouse Brain Atlas; <https://mouse.brain-map.org/static/atlas>) were selected and processed for hematoxylin and eosin staining. Coronal brain images were acquired in the NanoZoomer 2.0-HT slide scanner (Hamamatsu Photonics K.K.) using a 20 \times magnification. Corpus callosum thickness was measured using QuPath (University of Edinburgh) ImageJ software.

Statistics

All statistical tests were performed with Prism 6 (GraphPad Software). Specifically, for multiple comparisons, the 1-way analysis of variance statistical test was performed followed by Tukey's post hoc test. $P < .05$ was considered significant. Statistical tests and sample sizes are indicated in figure legends and significance was defined as $*P < .05$ and $**P < .01$.

Results

Variants in *ADD1* are associated with corpus callosum malformation and neurological symptoms

Case I-1 is a female from a consanguineous family, and she was diagnosed with ID/mental retardation (Supplemental Figure 1, Supplemental Table 3). At age 2 years, case I-1 showed ACC, abnormal sulcation of the medial cerebral hemispheres, and grossly enlarged lateral and third ventricles on brain magnetic resonance imaging (MRI) (Figure 1A, Supplemental Table 3). She also had hypoplasia of the white matter and the cerebellar vermis. Exome sequencing of case I-1 and her parents identified recessive variants in *ADD1* and *RTKN2* that were predicted to be damaging by Polymorphism Phenotyping v2 and Protein Variation Effect Analyzer (Supplemental Figure 1B-D). RNA sequencing data from the Genotype-Tissue Expression (GTEx) data set and other published data sets showed that *ADD1* but not *RTKN2* was expressed in adult or developing brain tissues (Supplemental Figure 1E-G). The rare recessive *ADD1* variant (Chr4:2877811A>T, hg19, p.Arg57Trp, Genome Aggregation Database (gnomAD) allele frequency 0/313396) (Figure 1B) was considered the best candidate for symptoms in case I-1.

Case II-1 is a female diagnosed with global developmental delay and ID. Case II-1 showed partial ACC at age 13 months, consisting of only a segment of the anterior body measuring approximately 2 cm (Figure 1A, Supplemental Table 3). There was abnormal lobulation and disorganized subluxation and folia of the inferior and lateral aspects of the left cerebellar hemisphere. The patient showed proportional stature, distinctive facial features, generalized hypotonia, and developed seizures controlled with a ketogenic diet. She

had a diagnosis of cerebral palsy and autism and continued to make progress with her speech. Exome sequencing of case II-1 and her parents helped in identifying a single rare de novo truncation variant in *ADD1* (Chr4:2906748_G>A, ADD1: NM_014189.3, c.1418G>A, p.Trp473*, not found in gnomAD) (Figure 1A and B).

Case III-1 is a female born at 40 weeks with normal weight, length, and head circumference (35 cm, 80th percentile) (Supplemental Table 3). She was noted in utero to have complete ACC, and a follow-up brain MRI on day 1 confirmed this. She was hypotonic with right hemiplegia and failed to thrive as an infant who required a g-tube for 12 months. She had mild motor delays. She sat independently at age 10 months and walked at age 14 months. She had a seizure of unclear origin at age 2 years 11 months, which was suspected to be related to hypernatremia. A subsequent electroencephalogram was normal. She also has had multiple staring spells that do not have an electroencephalogram correlate. A brain MRI performed at age 20 months noted complete ACC with absence of the cingulate gyrus and septum pellucidum (Figure 1A). There was an associated parallel configuration of the lateral ventricles with colpocephaly. The bilateral optic nerve sheath complexes were tortuous, and the optic nerves appeared slightly thin. She had a normal muscle biopsy at age 5 years with muscle coenzyme Q10 at 21.1 $\mu\text{g/g}$ (normal 24-33 $\mu\text{g/g}$). Muscle electron transport chain enzymology compared with controls noted a complex I deficiency of 26% and complex IV deficiency of 24%. She was started on ubiquinol with some improvement in her fatigue. Her other symptoms included patent foramen ovale, headaches, leg pains, night sweats, leukocytosis, and a qualitative platelet defect. At age 8 years, she continues to have gastrointestinal issues with constipation, fatigue, leg and joint pain, and staring spells. She has behavioral outbursts, sensory issues, and mild attention issues, and she continues to be on the low end of the growth curve for length (121.3 cm, eighth percentile) and weight (21 kg, sixth percentile). Reanalysis of clinical negative exome sequencing of case III-1 and her parents identified a rare de novo truncation variant in *ADD1* (Chr4:2930065-2930075 delGC-CAGCCCCGA, NM_001119, c.2029_2039del, p.Glu680Argfs*7, gnomAD allele frequency 0/251484) (Figure 1C) and a missense variant in *CLASPI* (Chr2:122218756_C>T, NM_015282, c.G953A, p.R318Q) of unknown significance.

Case IV-1 is a male and presented with seizures beginning at age 1 year, along with speech delay, mild ID, and attention deficit/hyperactivity disorder (ADHD). Brain imaging at age 3.5 years did not display noticeable structural abnormalities. Exome sequencing of case IV-1 and his parents identified a de novo missense variant in *ADD1* (Chr4:2896387_C>T, ADD1: NM_001119, c.670C>T, p.His224Tyr, gnomAD allele frequency 0/31320) (Figure 1C). This variant was predicted to be deleterious by Protein Variation Effect Analyzer (Supplemental Figure 1D). The only other variants identified in case IV-1

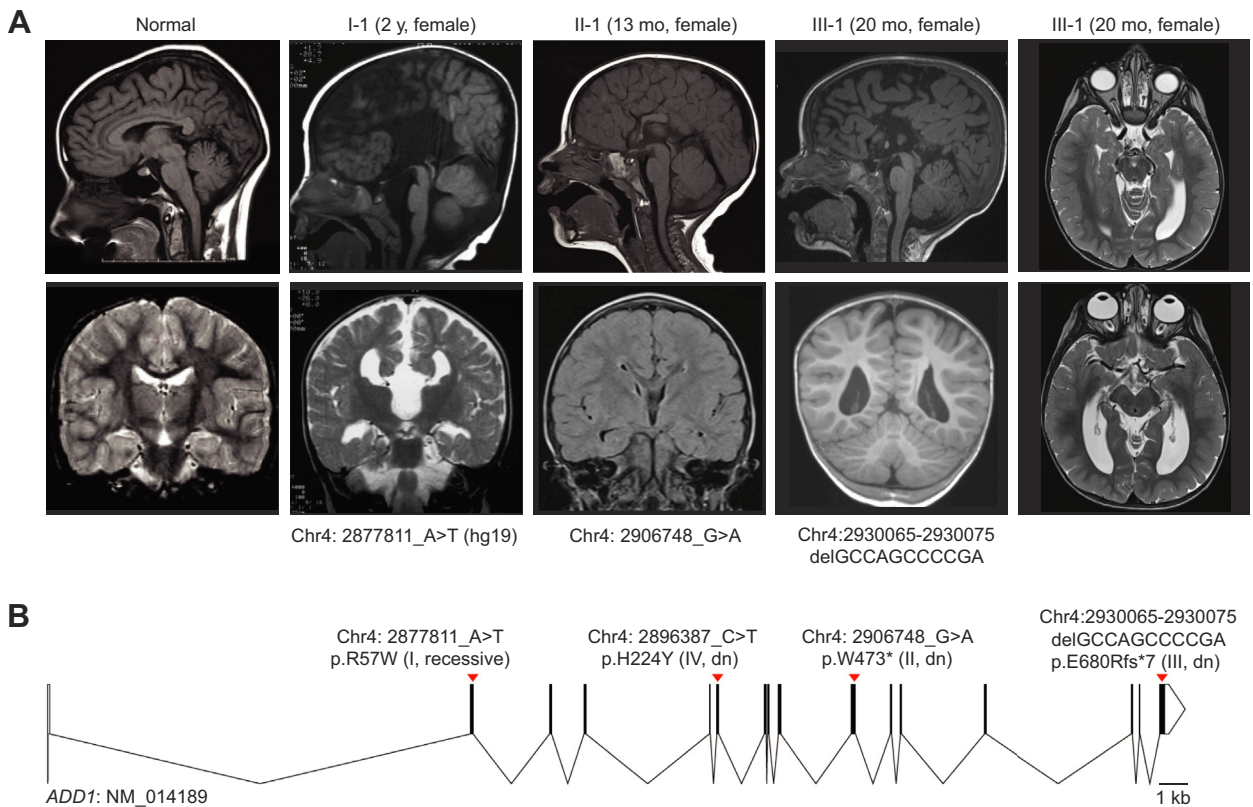


Figure 1 Variants in *ADD1* are associated with agenesis of corpus callosum (ACC) and ventriculomegaly. **A.** Brain magnetic resonance imaging showing that *ADD1* variants are associated with ACC. Case I-1 carrying the homozygous *ADD1* variant Chr4:2877811_A>T (hg19, p.Arg57Trp) exhibits ACC, a grossly enlarged third ventricle, and hypoplasia of the white matter and cerebellar vermis. Case II-1 carrying the de novo truncation variant Chr4:2906748_G>A (p. Trp473*, NM_014189) exhibits partial ACC with only a segment of the anterior body present; there is also abnormal lobulation and disorganized subluxation and folia of the inferior and lateral aspects of the left cerebellar hemisphere. Case III-1 carrying the de novo truncation variant Chr4:2930065-2930075 delGCCAGCCCCGA, NM_001119, p.Glu680Argfs*7 exhibits complete ACC and enlarged ventricles. **B.** *ADD1* exon–intron structure and the positions of variants reported in this study. See [Supplemental Figure 1](#) for further details. mo, month; y, year.

were compound heterozygous missense variants in *SPTBN2* (NM_003128 c.4022G >A p.Arg1341Gln, and c.1004A >G p.Asn335Ser), the spectrin beta nonerythrocytic 2/ β III-spectrin gene associated with spinocerebellar ataxia, although case IV-1 does not have ataxia.

Among the more than 120,000 whole exomes on gnomAD, zero homozygous *ADD1* LoF variants have been reported, and the total observed LoF alleles are 14% (90% CI, 7%-30%) of the expected (probability of being loss-of-function intolerant = 0.99),²⁵ indicating that *ADD1* is intolerant to LoF variants and that de novo damaging variants can be deleterious. We examined 54 deletion variants affecting the *ADD1* locus reported on ClinVar, and most of these deletions were associated with developmental delay. Interestingly, 1 deletion (hg19 chr4:71552-29006745) was associated with ventriculomegaly, ACC, Dandy-Walker malformation, and intrauterine growth retardation. Two additional deletions (hg38 chr4:36424-3881330, hg38 chr4:68453-6055026) were associated with microcephaly, delayed speech, muscular hypotonia, and motor delay. *ADD1* is located in Chr4p16.3, and the region is associated with Wolf-Hirschhorn syndrome. The variants reported in

this study support that recessive and de novo damaging *ADD1* variants are associated with brain malformations and neurological symptoms such as ID and attention deficit.

***ADD1* splicing isoforms are dynamically expressed during cortical development**

ADD1 messenger RNA (mRNA) was broadly expressed in human neural and nonneural tissues ([Supplemental Figure 1E](#)), whereas *ADD2* mRNA was expressed in the brain ([Supplemental Figure 2A](#)). We examined the impact of sex on *ADD1* expression using the GTEx data set²⁶ and did not find differential expression of *ADD1* between male and female brain tissues ([Supplemental Figure 1F](#)). RNA sequencing and RT-PCR results showed that *ADD1* mRNA was highly expressed in the developing human brain, and *ADD1* splicing isoforms were differentially expressed between the ventricular zone and cortical plate (CP) ([Figure 2A](#)). Specifically, exon 10 of human *ADD1* had an extended 5' splice site that was preferentially expressed in the CP, which mainly consists of postmitotic neurons; exon 15 was selectively included in the CP as well. RNA

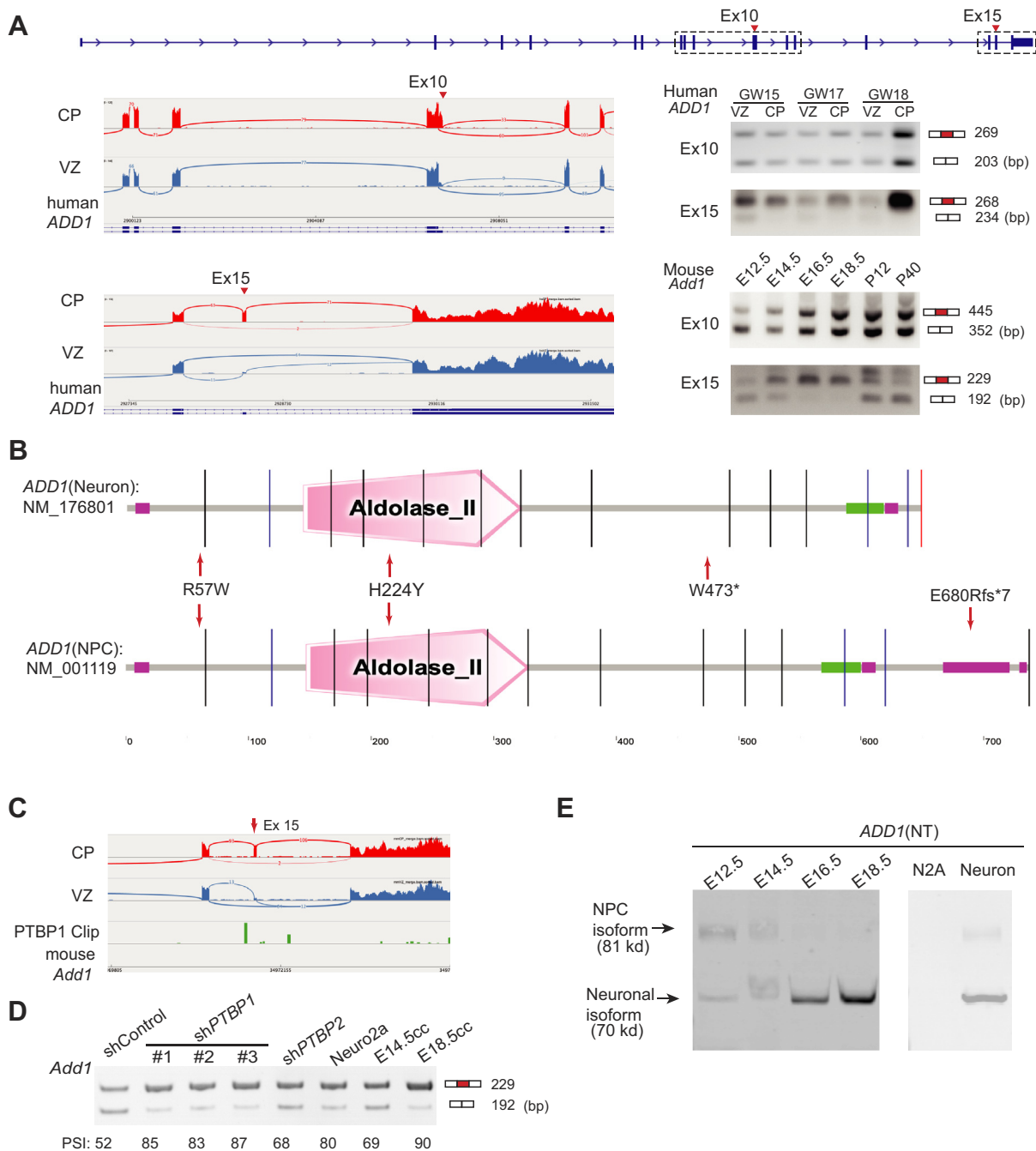


Figure 2 *ADD1* splicing isoforms are differentially expressed in the developing neocortex. **A**, Alternative splicing of *ADD1* Ex10 and Ex15 during human and mouse brain development. Top, genome (exon–intron) structure of *ADD1* with the positions of Ex10 and Ex15 indicated. Left, RNA sequencing results and Sashimi plots showing the alternative 5' splice site for Ex10 and the inclusion/exclusion of Ex15 between the CP (mostly neurons) and VZ (mostly NPCs) of GW13 to GW16 human fetal brains.⁴⁰ Top right, reverse transcriptase–polymerase chain reaction (RT-PCR) results showing that human *ADD1* Ex10 and Ex15 are differentially spliced between microdissected VZ and CP; Bottom right, RT-PCR results showing that mouse *Add1* Ex10 and Ex15 are differentially spliced during dorsal cortex development. **B**, *ADD1* splice isoforms between neurons (top, NM_176801) and NPCs (bottom, NM_001119). The neuronal isoform has a longer neck domain because of extended Ex10 but lacks the MARCKS-related domain because of inclusion of Ex15, which introduces an in-frame stop codon. Positions of variants reported in this study are indicated. **C**, CLIP-Seq peaks (green) showing that PTBP1 binds to *Add1* intron 14. **D**, RT-PCR results showing that *Ptp1* shRNAs promote inclusion of *Add1* Ex15 in Neuro2a cells. **E**, Western blot analysis of *ADD1* isoforms on E12.5, E14.5, E16.5, and E18.5 mouse dorsal brains, Neuro2a cells, and primary hippocampal neurons (DIV11). See [Supplemental Figure 2](#) for further details. bp, base pair; CLIP-Seq, cross-linking immunoprecipitation and sequencing; CP, cortical plate; DIV11, 11 days in vitro; E, embryonic day; Ex, exon; GW, gestation week; NPC, neural progenitor cell; NT, N terminal; PSI, percentage spliced in; sh, short hairpin; VZ, ventricular zone.

sequencing data from GTEx confirmed that *ADD1* isoform containing extended exon 10 and inserted exon 15 was specifically expressed in brain tissues (Supplemental Figure 2B). Hereafter, we refer to *ADD1* transcript NM_176801 with extended exon 10 and inclusion of exon 15 as the neuronal isoform and the *ADD1* transcript NM_001119 with shorter exon 10 and exclusion of exon 15 as the neural progenitor cell (NPC) isoform (Figure 2A and B).

Interestingly, the inclusion of exon 15 introduces an in-frame stop codon leading to the removal of the C-terminal MARCKS-related domain. Thus, the NPC isoform contains the MARCKS-related domain for localization to lateral membranes, whereas the neuronal isoform lacks this domain and has an extended neck domain (Figure 2B). *Add1* exon 10 and exon 15 were also differentially spliced in the developing mouse neocortex (Figure 2A, Supplemental Figure 2C).

The RNA binding protein PTBP1 is expressed in NPCs and suppresses neuronal exon insertion.^{21,27} The intronic sequence upstream of *Add1* exon 15 contains a CU-rich PTBP1 binding motif and bears a PTBP1 CLIP-Seq peak in NPCs (Figure 2C). We infected Neuro2a cells with shRNAs targeting *Ptbp1* and found that 3 different *Ptbp1* shRNAs significantly increased the inclusion of *Add1* exon 15 (neuronal isoform) (Figure 2D). Interestingly, other genes associated with adducins and β -spectrin, such as *Ank2* and *Epb4.1l3*, were differentially spliced during cortical neurogenesis and coordinately regulated by PTBP1 (Figure S2D). These results indicate that PTBP1 suppresses the *Add1* neuronal isoform during cortical neurogenesis.

We examined multiple antibodies to determine their specificity to adducin homologs and isoforms (Supplemental Figure 2E and F, Figures 2E and 3A). Two antibodies specifically recognized the ADD1 N-terminal domain (sc33633, named ADD1[NT] hereafter) or the ADD1 C-terminal domain (HPA035873, named ADD1[CT]) but not those of ADD2 and ADD3; another antibody (ab51130, pan-ADD) recognized the conserved C-terminal MARCKS-related domain shared by ADD1/ADD2/ADD3 (Supplemental Figure 2E and F). Western blotting with ADD1(NT) antibody confirmed that NPC and neuronal ADD1 protein isoforms were dynamically expressed during brain development (Figure 2E). On P7 in mice, adducins were expressed in the neocortex and highly enriched in callosal axons (Figure 3B, Supplemental Figure 3A). On E14.5, ADD1 and other adducins were expressed broadly in the brain and enriched in the cytosol (Figure 3C).

The lack of the C-terminal MARCKS-related domain in the tail of neuronal ADD1 suggests that previously-detected MPS signals with the pan-ADD antibody are likely ADD2 or ADD3 (Figure 2E, Supplemental Figure 2E and F).¹⁰ Thus, it remained unclear whether the ADD1 neuronal isoform is associated with the MPS. We examined endogenous and transfected ADD1 neuronal isoform in primary hippocampal neurons and found that

the ADD1 neuronal isoform was localized in the axons (Figure 3D and E). Next, we performed STED imaging by staining adducins with the pan-ADD antibody and ADD1-specific antibodies in primary cultured rat hippocampal neurons. Both the pan-ADD and ADD1-specific antibodies highlighted periodic structures, but the ADD1-specific antibodies showed a less distinct signal (Supplemental Figure 3B, Figure 3F and G). In summary, the ADD1 neuronal isoform is expressed in axons and associated with the MPS.

ADD1 variants disrupt protein expression and adducin dimerization

To determine the effect of *ADD1* variants on protein expression, we expressed *ADD1* NPCs and neuronal isoforms carrying the recessive variant (Chr4:2877811A>T, p.Arg57Trp) in Neuro2a cells. Although the protein level was not significantly affected, truncated protein products were observed when the p.Arg57Trp mutant was expressed in either the NPCs or neuronal isoforms (Figure 4A) suggesting that the p.Arg57Trp variant may lead to aberrant splicing or protein translation/cleavage. *Add1* mRNA level was significantly decreased in *Add1* heterozygous KO mice compared with wild-type mice,¹⁵ which strongly suggests the possibility of a dosage effect. To examine whether de novo truncation *ADD1* alleles affect protein expression, we generated *ADD1* heterozygous HEK293FT cells (*ADD1*^{+/-}) (Supplemental Figure 4A) and found that *ADD1*^{+/-} led to decreased ADD1 protein levels (Figure 4B). Our results indicate that the p.Arg57Trp missense and truncating *ADD1* variants affect ADD1 protein expression.

The N-terminal and C-terminal domains of ADD1 have been reported to mediate ADD1–ADD2 dimerization.²⁸ We expressed ADD1 mutant proteins and tested their efficiency in pulling down ADD2 through immunoprecipitation. We found that the missense variants (p.Arg57Trp and p.His224Tyr) in the head domain and the p.Trp473* truncation variant impaired ADD1–ADD2 interaction (Figure 4C–F). These results indicate that *ADD1* variants caused damaging effects by decreasing protein levels and/or disrupting adducin complex formation.

Add1 KO mice display ventriculomegaly and corpus callosum malformation

Homozygous *Add1* KO (*Add1*^{-/-}) mice have been reported to show lethal hydrocephalus at 50% penetrance,¹⁵ and axonal degeneration occurs in *Add1*^{-/-} optic nerves and dorsal root ganglion neurons.¹¹ In this study, we examined the lateral ventricles and formation of the corpus callosum in *Add1*^{-/-} mice that did not show lethal hydrocephalus (Figure 5, Supplemental Figure 5). *Add1*^{-/-} mice showed ventriculomegaly at neonatal, P14, and adult stages

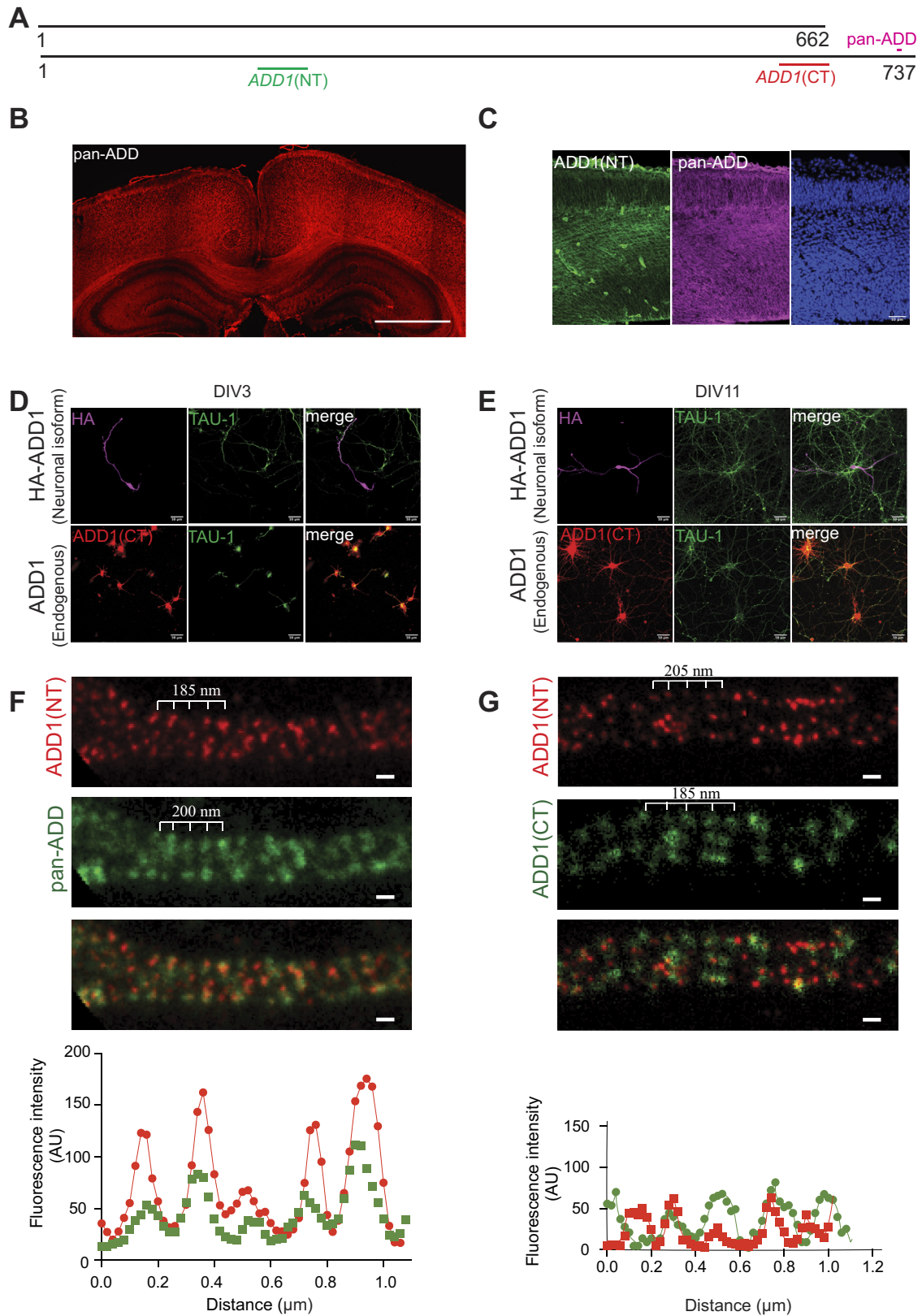


Figure 3 Expression of *ADD1* splice isoforms in the brain. **A**. Schematic structure of *ADD1* isoforms with regions that are recognized by different antibodies. *ADD1* (NT), sc33633; *ADD1* (CT), HPA035873; pan-ADD, ab51130. **B**. Immunostaining of postnatal day 7 mouse brain with pan-ADD antibody showing that adducins are expressed in the cortex and enriched in the corpus callosum. Scale bar = 1000 μm . **C**. Immunostaining of embryonic day 14.5 mouse cortex with pan-ADD and *ADD1*-specific antibody (*ADD1*[NT]) showing that *ADD1* is expressed in the developing mouse brain. **D**. Immunostaining of transfected and endogenous *ADD1* showing localization in axons of DIV3 primary mouse hippocampal neurons. **E**. Immunostaining of *ADD1* showing localization in axons of rat DIV11 primary hippocampal

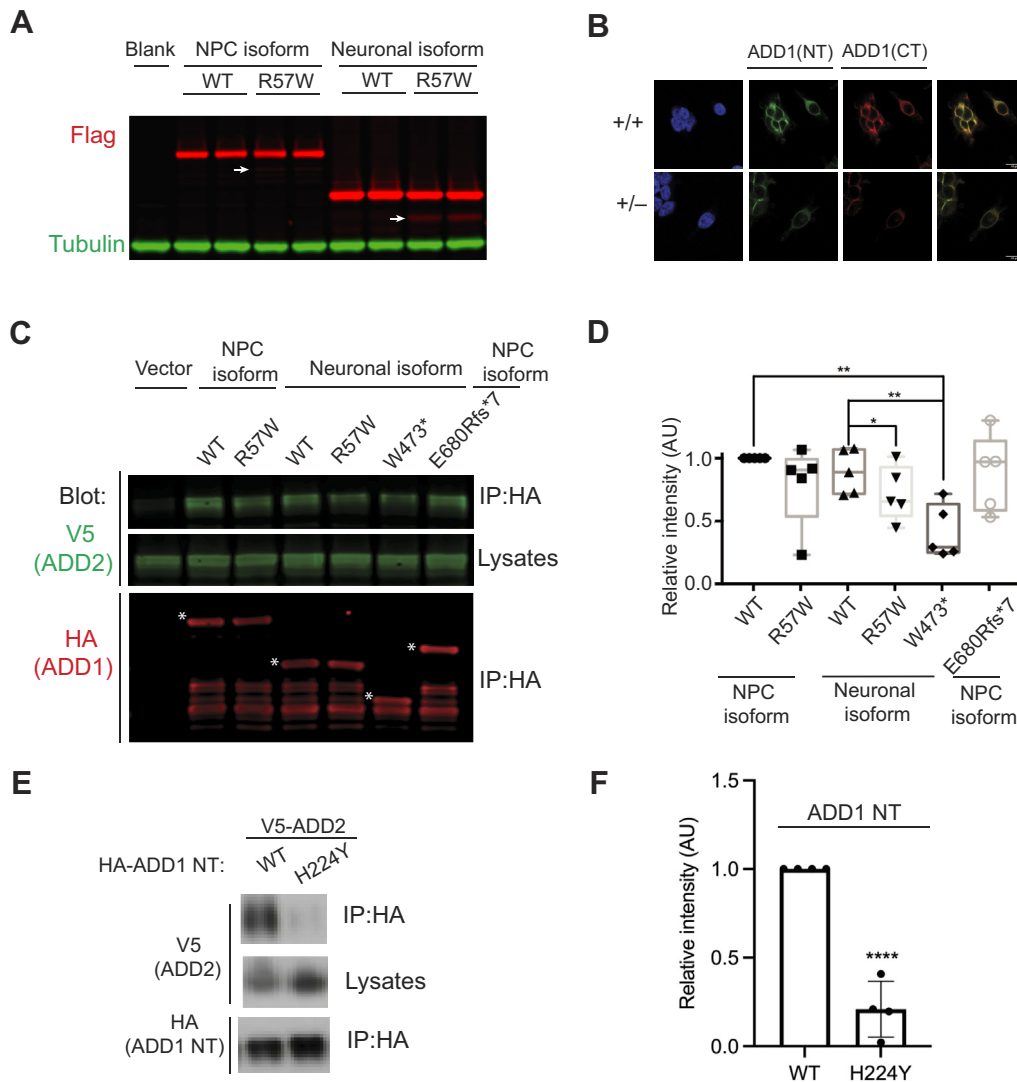


Figure 4 *ADD1* variants disrupt protein functions. **A**, Expression of the *ADD1* WT and mutant forms in Neuro2a cells, showing that the Chr4:2877811_A>T (hg19, p.R57W) variant leads to a noticeable number of truncated proteins (white arrows). **B**, Immunostaining results using antibodies against ADD1 NT (ADD1[NT]) (green) and CT (ADD1[CT]) (red) show reduced protein levels in *ADD1* heterozygous (\pm) HEK293FT cells. Scale bar, 20 μ m. **C**, Coimmunoprecipitation of V5-ADD2 transfected with indicated versions of HA-ADD1 (white stars) in HEK293FT cells showing that ADD1 p.R57W and p.W473* reduced ADD1-ADD2 protein interaction. **D**, Statistical analysis of signals in **C**. * $P < 0.05$, ** $P < 0.01$, t test. **E**, Coimmunoprecipitation of V5-ADD2 transfected with indicated versions of HA tagged ADD1 N-terminus (1-430 amino acids) in Neuro2a cells showing that p.H224Y reduced ADD1-ADD2 protein interaction. **F**, Statistical analysis of signals in **E**. **** $P < .0001$, t test. See [Supplemental Figure 4](#) for further details. AU, arbitrary unit; CT, C terminal; IP, immunoprecipitation; NPC, neural progenitor cell; NT, N terminal; WT, wild type.

([Figure 5A](#), [Supplemental Figure 5A](#)). In 9-week-old *Add1*^{-/-} mice, the thickness of the corpus callosum was significantly decreased in the rostral brain when compared with *Add1*^{+/+} littermates ($n = 3$ animals; $P < .01$); the corpus callosum in *Add1*^{+/-} heterozygotes appeared thinner, but this was not statistically significant. In the caudal brain,

the thickness of corpus callosum was significantly decreased in *Add1*^{-/-} samples ([Figure 5A-C](#)). On P0 and P14, the corpus callosum also showed a trend of thinning in *Add1*^{-/-} mice ([Supplemental Figure 5A-D](#)). These results indicate that deletion of *Add1* is associated with ventriculomegaly and corpus callosum degeneration in mice.

neurons. **F**, Stimulated emission depletion (STED) imaging of ADD1 isoforms in primary cultured rat hippocampal neurons showing periodic signals of ADD1(ADD1[NT]) and pan-adducins (pan-ADD) in the axon. Scale bar = 0.2 μ m. **G**, STED imaging of ADD1 isoforms in primary cultured rat hippocampal neurons showing periodic signals of ADD1 (ADD1[NT], ADD1[CT]) in the axon. Scale bar = 0.2 μ m. See [Supplemental Figure 3](#) for further details. AU, arbitrary unit; CT, C terminal; DIV3, 3 days in vitro; DIV11, 11 days in vitro; NT, N terminal.

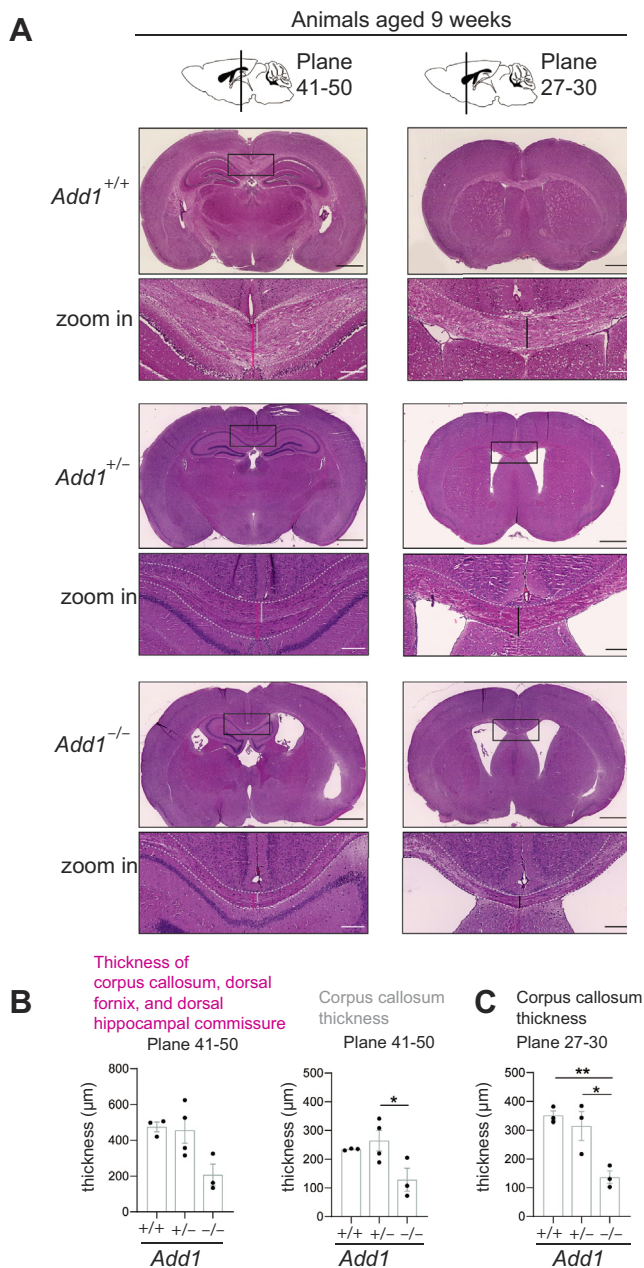


Figure 5 Corpus callosum thickness is decreased in adult mice in the absence of *Add1*. **A**. Hematoxylin and eosin staining of brain coronal sections from adult wild-type (*Add1*^{+/+}), heterozygous (*Add1*^{+/-}), and knockout (*Add1*^{-/-}) *Add1* animals. Scale bar = 500 µm; zoom-in scale bar = 100 µm. **B**. Quantification of the thickness of the corpus callosum, dorsal fornix, and dorsal hippocampal commissure (indicated by pink lines in **A**) and of corpus callosum only (indicated by gray lines in **A**) in coronal brain plates 41 to 50. Data represent mean ± SEM ($n = 3-4$ animals per condition). * $P < .05$ by 1-way analysis of variance (ANOVA) with Tukey's post hoc test. **C**. Quantification of corpus callosum thickness (indicated by black lines in **A**) in coronal brain plates 27 to 30. Data represent mean ± SEM ($n = 3$ animals per condition). * $P < .05$, ** $P < .01$ by 1-way ANOVA with Tukey's post hoc test. See Supplemental Figure 5 for further details.

Discussion

Our results show that *ADD1* is differentially spliced during neurogenesis, and LoF variants in *ADD1* are associated with corpus callosum malformation, ventriculomegaly, ID, and attention deficit. *Add1* KO mice showed absence/degeneration of the corpus callosum and lethal ventriculomegaly (ie, hydrocephalus), highly similar to the affected individual with the recessive *ADD1* variant. Furthermore, we showed that missense and de novo variants in *ADD1* impair *ADD1*–*ADD2* dimerization and decrease *ADD1* levels. These data provide strong support that LoF variants in *ADD1* cause malformations of the corpus callosum, ventriculomegaly, and neurological symptoms in humans.

Among the 4 variants reported in this study, the recessive missense variants p.Arg57Trp and p.His224Tyr fall in the core (head and neck) domain of *ADD1*, which mediates oligomerization.²⁸ Consistent with this, we found that the p.Arg57Trp and p.His224Tyr variants weakened the association of *ADD1* with *ADD2* (Figure 4). The tail domain of *ADD1* has also been reported to regulate dimerization,¹² and the de novo truncation variant p.Trp473* significantly reduced the association between *ADD1* and *ADD2*. It was intriguing that de novo variants in *ADD1* caused variable but closely related neurological symptoms compared with the recessive variant. We noticed that *Add1* mRNA levels were decreased in *Add1*^{+/-} mice¹⁵ and hypothesized that the heterozygous *ADD1* variants had dosage effects. Heterozygous human cells harboring premature stop codons indeed decreased *ADD1* protein levels (Figure 4B), suggesting that de novo truncating variants led to reduced amounts of *ADD1* protein. Interestingly, the *ADD1* truncation variant affecting only the neuronal isoform (case II-1, p.Trp473*) was associated with ACC but not with ventriculomegaly, whereas the *ADD1* truncation affecting only the NPC isoform (case III-1, p.Glu680Argfs*7) was associated with both ACC and ventriculomegaly (Figures 1A and 2B), suggesting that ventriculomegaly relates to the function of *ADD1* NPC isoform.

Adducins promote the assembly of β -spectrin and actin,^{29,30} and in neurons, adducins form the MPS with actin and β -spectrin tetramers.¹⁰ Previously, we showed that *Add1* KO led to increased diameters of MPS rings and axonal degeneration.¹¹ Our current work in humans and KO mice suggests that *ADD1* is required in the brain for balancing cerebrospinal fluid and maintaining intact axon structure. Interestingly, neonatal β II-spectrin gene *Sptbn1* KO mice displayed completely absent or significantly diminished interhemispheric axonal bundles including the corpus callosum, whereas juvenile β II-spectrin gene *Sptbn1* mutants showed a significant increase in the diameter of myelinated axons and signs of axonal degeneration.³¹ Very recently, dominant variants in β II-spectrin *SPTBN1* were associated

with a neurodevelopmental syndrome.³² Thus, the adducin- β -spectrin complex plays an essential role in the mouse and human brain development.

Ankyrins anchor proteins such as ion channels to the spectrin-actin-based membrane cytoskeleton through direct interaction with spectrin tetramers.⁶ In neurons, the levels of AnkyrinB/ANK2 and β II-spectrin/SPTBN1 critically regulate MPS formation in axon development.³³ Loss of β II-spectrin led to decreased ANK2 levels in mice, and de novo LoF variants in the *ANK2* gene have been repeatedly associated with autism in human genetics studies.³⁴ Consistent with the *ANK2* LoF phenotype, case IV-1 carrying a de novo *ADD1* missense variant displayed speech delay, mild ID, and ADHD. The association of *ADD1* truncation variants with structural brain malformation, and the association of the missense *ADD1* variant with mild ID and ADHD suggest that *ADD1* protein dosage is critical for neurological functions. This is consistent with the pleiotropic hydrocephalus and axonal degeneration phenotypes observed in *Add1* KO mice (Figure 5).¹¹ These observations suggest that variants in components of the adducin-actin-spectrin-ankyrin cytoskeleton network can cause dosage-dependent and pleiotropic neurological symptoms.

Adducins associate with β -spectrin through their C-terminal conserved MARCKS-related domain,¹² and a pan-adducin antibody (ab51130) against this conserved domain showed MPS in axons.¹⁰ Given that the pan-adducin antibody recognizes *ADD1*, *ADD2*, and *ADD3* (Supplemental Figure 2F), it was unclear which adducin(s) was associated with the MPS, let alone which splice isoform. In this study, we show that *ADD1* undergoes alternative splicing between NPCs and neurons and that the neuronal isoform lacks the conserved MARCKS-related domain (Figure 2). Our data suggest that although *ADD1* was expressed in neuronal axons, the previously reported signal using the pan-ADD antibody was probably from *ADD2* and/or *ADD3*. Intriguingly, our super-resolution imaging using STED showed that the truncated neuronal *ADD1* isoform was still associated with the MPS, implying that the C-terminal MARCKS-related domain is not required for *ADD1*'s association with the MPS.

Alternative splicing of neuronal genes has been increasingly associated with neurological disorders.³⁵ In this study, we show that *Add1* is differentially spliced during cortical neurogenesis; the neuronal isoform lacks the C-terminal MARCKS-related domain and is suppressed by PTBP1 in NPCs. Interestingly, our current and previous work showed that *Ank2*, *Epb4.111*, *Epb4.113*, and *Tpm2* were also coordinately and differentially spliced during brain development (Supplemental Figure 2D).²¹ Furthermore, *Ptbp1* KO mice displayed a lethal hydrocephalus phenotype³⁶ that is comparable with *Add1* KOs, suggesting that PTBP1-mediated splicing of *Add1* has physiological consequences. Together, these observations suggest that the adducin-actin-spectrin-ankyrin cytoskeletal protein network undergoes coordinated alternative splicing during neurogenesis and neuronal differentiation, thereby promoting the

restructuring of the membrane cytoskeleton from a polygonal scaffold to the ring-like MPS in neurons.

Common adducin genetic variants were associated with cognitive deficiency in schizophrenia,³⁷ and mixed evidence showed that polymorphisms in *ADD1*, especially p.Gly460Trp, were associated with essential hypertension³⁸ and cardiovascular disease in individuals with hypertension.³⁹ Interestingly, the cases reported here showed developmental delay (II-1) and symptoms in other tissues such as persistent ketoacidosis, lactic acidosis, and a qualitative platelet defect (III-1, Supplemental Table 3). *ADD1* is expressed in the heart, brain, and broadly in other human tissues (Supplemental Figure 1E), and deletion of *Add1* in mice causes compensated hemolytic anemia.¹⁵ These observations suggest that *ADD1* may have essential functions in other tissues in addition to the brain. Further studies are required to gain a complete understanding of *ADD1* variant-related clinical presentations.

Data Availability

Under institutional privacy policies and institutional review boards, further data and experimental details are available upon request.

Acknowledgments

We would like to thank Prof Soma Das for insightful comments on the manuscript, all the affected individuals and families in this study, and Dr Nahit Motavalli Mukaddes for referring cases. The Genotype-Tissue Expression (GTEx) Project was supported by the Common Fund of the Office of the Director of the National Institutes of Health and by the National Cancer Institute, National Human Genome Research Institute, National Heart, Lung, and Blood Institute, National Institute on Drug Abuse, National Institute of Mental Health, and National Institute of Neurological Disorders and Stroke. This work was supported by grants from the National Institute of Mental Health (K01 MH109747) and National Institute of General Medical Sciences (DP2 GM137423) to X.Z. and by the Manton Center for Orphan Disease Research and grants from National Institute of Neurological Disorders and Stroke (R01 NS035129 and R01 NS032457) to C.A.W. C.A.W. is a distinguished investigator of the Paul G. Allen Family Foundation and an investigator of the Howard Hughes Medical Institute. M.M.S is supported by Fundo Europeu de Desenvolvimento Regional through the Norte Portugal Regional Operational Programme, Portugal 2020, and by FCT - Fundação para a Ciência e a Tecnologia/Ministério da Ciência, Tecnologia e Ensino Superior (NORTE-01-0145-FEDER-028623; PTDC/MED-NEU/28623/2017). C.F. was supported by the Region of Southern Denmark.

Author Information

The patient information was collected at Boston Children's Hospital, University of Alberta, The Children's Hospital of Philadelphia, and Odense University Hospital. O.C., R.D.G., C.B.A., C.F., C.B., E.J.B., L.K.H., C.C.M., M.J.F., H.H., K.T.K., and J.E.N. reviewed the clinical information. C.Q., I.F., A.R.C., R.P.C., D.L., R.S.H., X.R., B.K., K.H., R.Z., P.B., and X.Z. performed experiments and data analyses. C.A.W., M.M.S., and X.Z. supervised the research. C.Q., I.F., and X.Z. wrote the manuscript, and C.Q., I.F., A.R.C., R.P.C., J.E.N., O.C., D.L., R.D.G., C.B.A., C.F., L.K.H., C.B., C.C.M., X.R., B.K., K.H., R.Z., P.B., E.J.B., R.S.H., M.J.F., H.H., K.T.K., M.M.S., C.A.W., and X.Z. commented on it.

Ethics Declaration

This study was conducted with the approval of institutional review boards and according to the ethical standards of the following participating institutions: Boston Children's Hospital, Boston; The Children's Hospital of Philadelphia, Philadelphia; University of Alberta, Edmonton; and Helen DeVos Children's Hospital, Grand Rapids ([Supplemental Table 1](#)). Informed consent was obtained from all subjects involved in this study or from parents of those who were aged <18 years. Control postmortem human tissues were obtained from NIH NeuroBioBank (<https://neurobiobank.nih.gov/about-best-practices/>). The protocols described were approved by of the University of Chicago Institutional Animal Care and Use Committee and/or the IBMC Ethical Committee and by the Portuguese Veterinarian Board.

Conflict of Interest

R.D.G. receives consulting fees from Minovia Therapeutics. All other authors declare no conflicts of interest.

Additional Information

The online version of this article (<https://doi.org/10.1016/j.gim.2021.09.014>) contains supplementary material, which is available to authorized users.

Affiliations

¹Department of Human Genetics, The University of Chicago, Chicago, IL; ²Nerve Regeneration Group, Instituto de Biologia Molecular e Celular (IBMC) and Instituto de Inovação e Investigação em Saúde, University of Porto, Porto, Portugal; ³Division of Genetics and Genomics and

Howard Hughes Medical Institute, Boston Children's Hospital, Departments of Pediatrics and Neurology, Harvard Medical School, Boston, MA; ⁴Department of Medical Genetics, Faculty of Medicine & Dentistry, University of Alberta, Edmonton, Alberta, Canada; ⁵Center for Applied Genomics, The Joseph Stokes Jr Research Institute, The Children's Hospital of Philadelphia, Philadelphia, PA; ⁶Mitochondrial Medicine Frontier Program, Division of Human Genetics, The Children's Hospital of Philadelphia, Philadelphia, PA; ⁷Department of Pediatrics, The Children's Hospital of Philadelphia, Perelman School of Medicine, University of Pennsylvania, Philadelphia, PA; ⁸Department of Clinical Genetics, Odense University Hospital, Odense, Denmark; ⁹Medical Genetics, Helen DeVos Children's Hospital, Grand Rapids, MI; ¹⁰Neurolipid Biology, Instituto de Inovação e Investigação em Saúde, and Instituto de Biologia Molecular e Celular (IBMC), University of Porto, Porto, Portugal; ¹¹Departments of Neurosurgery, Pediatrics, and Cellular & Molecular Physiology, Yale School of Medicine, New Haven, CT; ¹²The Neuroscience Institute, The University of Chicago, Chicago, IL

References

1. Paul LK, Brown WS, Adolphs R, et al. Agenesis of the corpus callosum: genetic, developmental and functional aspects of connectivity. *Nat Rev Neurosci.* 2007;8(4):287–299. <http://doi.org/10.1038/nrn2107>.
2. Edwards TJ, Sherr EH, Barkovich AJ, Richards LJ. Clinical, genetic and imaging findings identify new causes for corpus callosum development syndromes. *Brain.* 2014;137(Pt 6):1579–1613. <http://doi.org/10.1093/brain/awt358>.
3. Richards LJ, Plachez C, Ren T. Mechanisms regulating the development of the corpus callosum and its agenesis in mouse and human. *Clin Genet.* 2004;66(4):276–289. <http://doi.org/10.1111/j.1399-0004.2004.00354.x>.
4. Jeret JS, Serur D, Wisniewski K, Fisch C. Frequency of agenesis of the corpus callosum in the developmentally disabled population as determined by computerized tomography. *Pediatr Neurosci.* 1985;12(2):101–103. <http://doi.org/10.1159/000120229>.
5. Parrini E, Conti V, Dobyns WB, Guerrini R. Genetic basis of brain malformations. *Mol Syndromol.* 2016;7(4):220–233. <http://doi.org/10.1159/000448639>.
6. Bennett V, Baines AJ. Spectrin and ankyrin-based pathways: metazoan inventions for integrating cells into tissues. *Physiol Rev.* 2001;81(3):1353–1392. <http://doi.org/10.1152/physrev.2001.81.3.1353>.
7. Matsuoka Y, Li X, Bennett V. Adducin: structure, function and regulation. *Cell Mol Life Sci.* 2000;57(6):884–895. <http://doi.org/10.1007/PL00000731>.
8. Bennett V, Gilligan DM. The spectrin-based membrane skeleton and micron-scale organization of the plasma membrane. *Annu Rev Cell Biol.* 1993;9:27–66. <http://doi.org/10.1146/annurev.cb.09.110193.000331>.
9. Pan L, Yan R, Li W, Xu K. Super-resolution microscopy reveals the native ultrastructure of the erythrocyte cytoskeleton. *Cell Rep.* 2018;22(5):1151–1158. <http://doi.org/10.1016/j.celrep.2017.12.107>.
10. Xu K, Zhong G, Zhuang X. Actin, spectrin, and associated proteins form a periodic cytoskeletal structure in axons. *Science.* 2013;339(6118):452–456. <http://doi.org/10.1126/science.1232251>.
11. Leite SC, Sampaio P, Sousa VF, et al. The actin-binding protein α -adducin is required for maintaining axon diameter. *Cell Rep.* 2016;15(3):490–498. <http://doi.org/10.1016/j.celrep.2016.03.047>.
12. Hughes CA, Bennett V. Adducin: a physical model with implications for function in assembly of spectrin-actin complexes. *J Biol Chem.*

- 1995;270(32):18990–18996. <http://doi.org/10.1074/jbc.270.32.18990>.
13. Abdi KM, Bennett V. Adducin promotes micrometer-scale organization of beta2-spectrin in lateral membranes of bronchial epithelial cells. *Mol Biol Cell*. 2008;19(2):536–545. <http://doi.org/10.1091/mbc.e07-08-0818>.
14. Li X, Matsuoka Y, Bennett V. Adducin preferentially recruits spectrin to the fast growing ends of actin filaments in a complex requiring the MARCKS-related domain and a newly defined oligomerization domain. *J Biol Chem*. 1998;273(30):19329–19338. <http://doi.org/10.1074/jbc.273.30.19329>.
15. Robledo RF, Ciciotte SL, Gwynn B, et al. Targeted deletion of alpha-adducin results in absent beta- and gamma-adducin, compensated hemolytic anemia, and lethal hydrocephalus in mice. *Blood*. 2008;112(10):4298–4307. <http://doi.org/10.1182/blood-2008-05-156000>.
16. Vukojevic V, Gschwind L, Vogler C, et al. A role for α -adducin (ADD-1) in nematode and human memory. *EMBO J*. 2012;31(6):1453–1466. <http://doi.org/10.1038/emboj.2012.14>.
17. Gilligan DM, Lozovatsky L, Gwynn B, Brugnara C, Mohandas N, Peters LL. Targeted disruption of the beta adducin gene (Add2) causes red blood cell spherocytosis in mice. *Proc Natl Acad Sci U S A*. 1999;96(19):10717–10722. <http://doi.org/10.1073/pnas.96.19.10717>.
18. Yaguchi H, Yabe I, Takahashi H, et al. Sez612 regulates phosphorylation of ADD and neurogenesis. *Biochem Biophys Res Commun*. 2017;494(1-2):234–241. <http://doi.org/10.1016/j.bbrc.2017.10.047>.
19. Bednarek E, Caroni P. β -Adducin is required for stable assembly of new synapses and improved memory upon environmental enrichment. *Neuron*. 2011;69(6):1132–1146. <http://doi.org/10.1016/j.neuron.2011.02.034>.
20. Ruediger S, Vittori C, Bednarek E, et al. Learning-related feedforward inhibitory connectivity growth required for memory precision. *Nature*. 2011;473(7348):514–518. <http://doi.org/10.1038/nature09946>.
21. Zhang X, Chen MH, Wu X, et al. Cell-type-specific alternative splicing governs cell fate in the developing cerebral cortex. *Cell*. 2016;166(5):1147–1162.e15. <http://doi.org/10.1016/j.cell.2016.07.025>.
22. Fietz SA, Lachmann R, Brandl H, et al. Transcriptomes of germinal zones of human and mouse fetal neocortex suggest a role of extracellular matrix in progenitor self-renewal. *Proc Natl Acad Sci U S A*. 2012;109(29):11836–11841. <http://doi.org/10.1073/pnas.1209647109>.
23. Robinson JT, Thorvaldsdóttir H, Winckler W, et al. Integrative genomics viewer. *Nat Biotechnol*. 2011;29(1):24–26. <http://doi.org/10.1038/nbt.1754>.
24. Kaech S, Banker G. Culturing hippocampal neurons. *Nat Protoc*. 2006;1(5):2406–2415. <http://doi.org/10.1038/nprot.2006.356>.
25. Lek M, Karczewski KJ, Minikel EV, et al. Analysis of protein-coding genetic variation in 60,706 humans. *Nature*. 2016;536(7616):285–291. <http://doi.org/10.1038/nature19057>.
26. Oliva M, Muñoz-Aguirre M, Kim-Hellmuth S, et al. The impact of sex on gene expression across human tissues. *Science*. 2020;369(6509):eaba3066. <http://doi.org/10.1126/science.aba3066>.
27. Vuong CK, Black DL, Zheng S. The neurogenetics of alternative splicing. *Nat Rev Neurosci*. 2016;17(5):265–281. <http://doi.org/10.1038/nrn.2016.27>.
28. Joshi R, Bennett V. Mapping the domain structure of human erythrocyte adducin. *J Biol Chem*. 1990;265(22):13130–13136.
29. Mische SM, Mooseker MS, Morrow JS. Erythrocyte adducin: a calmodulin-regulated actin-bundling protein that stimulates spectrin-actin binding. *J Cell Biol*. 1987;105(6 Pt 1):2837–2845. <http://doi.org/10.1083/jcb.105.6.2837>.
30. Gardner K, Bennett V. Modulation of spectrin-actin assembly by erythrocyte adducin. *Nature*. 1987;328(6128):359–362. <http://doi.org/10.1038/328359a0>.
31. Lorenzo DN, Badea A, Zhou R, Mohler PJ, Zhuang X, Bennett V. β II-spectrin promotes mouse brain connectivity through stabilizing axonal plasma membranes and enabling axonal organelle transport. *Proc Natl Acad Sci U S A*. 2019;116(31):15686–15695. <http://doi.org/10.1073/pnas.1820649116>.
32. Cousin MA, Creighton BA, Breau KA, et al. Pathogenic SPTBN1 variants cause an autosomal dominant neurodevelopmental syndrome. *Nat Genet*. 2021;53(7):1006–1021. <http://doi.org/10.1038/s41588-021-00886-z>.
33. Zhong G, He J, Zhou R, et al. Developmental mechanism of the periodic membrane skeleton in axons. *eLife*. 2014;3:e04581. <http://doi.org/10.7554/eLife.04581>.
34. Iossifov I, Ronemus M, Levy D, et al. De novo gene disruptions in children on the autistic spectrum. *Neuron*. 2012;74(2):285–299. <http://doi.org/10.1016/j.neuron.2012.04.009>.
35. Parikshak NN, Swarup V, Belgard TG, et al. Genome-wide changes in lncRNA, splicing, and regional gene expression patterns in autism. *Nature*. 2016;540(7633):423–427. Published correction appears in *Nature*. 2018;560(7718):E30. <https://doi.org/10.1038/nature20612>.
36. Shibasaki T, Tokunaga A, Sakamoto R, et al. PTB deficiency causes the loss of adherens junctions in the dorsal telencephalon and leads to lethal hydrocephalus. *Cereb Cortex*. 2013;23(8):1824–1835. <http://doi.org/10.1093/cercor/bhs161>.
37. Bosia M, Pignoni A, Zagato L, et al. ADDing a piece to the puzzle of cognition in schizophrenia. *Eur J Med Genet*. 2016;59(1):26–31. <http://doi.org/10.1016/j.ejmg.2015.12.012>.
38. Cusi D, Barlassina C, Azzani T, et al. Polymorphisms of alpha-adducin and salt sensitivity in patients with essential hypertension. *Lancet*. 1997;349(9062):1353–1357. Published correction appears in *Lancet*. 1997;350(9076):524. [https://doi.org/10.1016/S0140-6736\(97\)01029-5](https://doi.org/10.1016/S0140-6736(97)01029-5).
39. Morrison AC, Bray MS, Folsom AR, Boerwinkle E. ADD1 460W allele associated with cardiovascular disease in hypertensive individuals. *Hypertension*. 2002;39(6):1053–1057. <http://doi.org/10.1161/01.hyp.0000019128.94483.3a>.
40. Camp JG, Badsha F, Florio M, et al. Human cerebral organoids recapitulate gene expression programs of fetal neocortex development. *Proc Natl Acad Sci U S A*. 2015;112(51):15672–15677. <http://doi.org/10.1073/pnas.1520760112>.